Remote Sensing of Environment 235 (2019) 111474

Contents lists available at ScienceDirect

Remote Sensing of Environment

journal homepage: www.elsevier.com/locate/rse

Variability of wood properties using airborne and terrestrial laser scanning

Jiri Pyörälä[a,b,c,*], Ninni Saarinen[a,c,d], Ville Kankare[d,a,c], Nicholas C. Coops[e], Xinlian Liang[b,c], Yunsheng Wang[b,c], Markus Holopainen[a,c], Juha Hyyppä[b,c], Mikko Vastaranta[d,c]

[a] Department of Forest Sciences, University of Helsinki, P.O Box 27, Helsinki, 00014, Finland
[b] Department of Remote Sensing and Photogrammetry, Finnish Geospatial Research Institute, Geodeetinrinne 2, Masala, 02431, Finland
[c] Center of Excellence in Laser Scanning Research, Finnish Geospatial Research Institute, Geodeetinrinne 2, Masala, 02431, Finland
[d] School of Forest Science, University of Eastern Finland, P.O. Box 111, Joensuu, 80101, Finland
[e] Department of Forest Resources Management, University of British Columbia, 2424, Main Mall, Vancouver, BC, V6T 1Z4, Canada

ARTICLE INFO

Keywords:
Lidar
Data fusion
Precision forestry
Scots pine

ABSTRACT

Information on wood properties is crucial in estimating wood quality and forest biomass and thus developing the precision and sustainability of forest management and use. However, wood properties are highly variable between and within trees due to the complexity of wood formation. Therefore, tree-specific field references and spatially transferable models are required to capture the variability of wood quality and forest biomass at multiple scales, entailing high-resolution terrestrial and aerial remote sensing methods. Here, we aimed at identifying select tree traits that indicate wood properties (i.e. wood quality indicators) with a combination of terrestrial laser scanning (TLS) and airborne laser scanning (ALS) in an examination of 27 even-aged, managed Scots pine (*Pinus sylvestris* L.) stands in southern Finland. We derived the wood quality indicators from tree models sampled systematically from TLS data and built prediction models with respect to individual crown features delineated from ALS data. The models were incapable of predicting explicit branching parameters (height of the lowest dead branch $R^2 = 0.25$, maximum branch diameter $R^2 = 0.03$) but were suited to predicting stem and crown dimensions from stand, tree, and competition factors (diameter at breast height and sawlog volume $R^2 = 0.5$, and live crown base height $R^2 = 0.4$). We were able to identify the effect of canopy closure on crown longevity and stem growth, which are pivotal to the variability of several wood properties in managed forests. We discussed how the fusions of high-resolution remote sensing methods may be used to enhance sustainable management and use of natural resources in the changing environment.

1. Introduction

The biodiversity and resilience of intensively managed forests are declining globally, leading to forest degradation in some regions (Hosonuma et al., 2012; Liang et al., 2016a; Sasaki and Putz, 2009). The argumentation for intensive forest management is mostly economical, i.e., high volume yields are desired in short rotations (Jokela et al., 2010). However, studies from four decades of species as diverse as, e.g., Scots pine (*Pinus sylvestris* L.), radiata pine (*P. radiata* D. Don), Norway spruce (*Picea abies* (L.) H. Karst.) and European beech (*Fagus sylvatica* L.) across several ecoregions suggest intensive forest management practices have reduced wood quality by affecting several influential wood properties, such as wood density, microfibril angle and tracheid dimensions (Macdonald and Hubert, 2002; Moore and Cown, 2017; Zhang, 1995; Zobel, 1984), adding to the similar effects induced by rising temperatures (Pretzsch et al., 2018). Namely, accelerated growth rates accompanied by short rotations has resulted in an increase in the proportion of juvenile wood and knots in wood. In addition to decelerating the rate of carbon sequestration in forests, reducing wood quality limit the use of timber in long-term carbon-binding applications in construction which would be central to the carbon balance of wood-based industries (Haus, 2018; Sterman et al., 2018). These multifaceted problems associated with intensive forest management in the changing environment could be better understood by utilizing the increasingly available remote sensing data to account for the variability of wood properties in the planning of forest management and industrial wood procurement. Bringing together a range of remote sensing datasets, methods and analysis techniques is key part of the transition to next-generation precision forestry that is required to tackle the various challenges associated with the unsustainable use of natural resources (Vauhkonen and Packalen, 2018; Xu et al., 2018).

Wood properties that determine wood quality (e.g. wood density,

* Corresponding author. Department of Forest Sciences, University of Helsinki, P.O Box 27, Helsinki, 00014, Finland.
E-mail address: jiri.pyorala@helsinki.fi (J. Pyörälä).

https://doi.org/10.1016/j.rse.2019.111474
Received 20 May 2019; Received in revised form 19 September 2019; Accepted 13 October 2019
Available online 26 October 2019
0034-4257/ © 2019 The Authors. Published by Elsevier Inc. This is an open access article under the CC BY license (http://creativecommons.org/licenses/BY/4.0/).

microfibril angle and tracheid dimensions) are the result of tree growth and wood formation. Many wood formation processes are dependent on cambial and apical age, and tree height and stem diameter, but are also variable with respect to environmental and genetic factors (Lundqvist et al., 2018; Rathgeber et al., 2016; Zobel and Jett, 2012). The tree apex and crown are the interfaces between the tree and the environment that act as regulators of growth by hormonally inducing cambial responses in the stem (i.e. wood formation) to changing conditions and tree structure (Sorce et al., 2013). One of the major implications includes that juvenile wood with high earlywood content, low wood density and steep microfibril angles is produced in young parts of stems (i.e. within the live crown). Crown morphology, i.e. size and vigor are related to wood properties and wood quality due to their relationship with the maturation of wood (Kuprevicius et al., 2013; Mansfield et al., 2007).

In forestry, wood quality indicators are used to describe elements that influence wood formation and the resulting wood properties: environmental factors such as growing stock density and soil fertility (Auty et al., 2018; Huuskonen et al., 2014; Mäkinen, 1999; Moore et al., 2009; Weiskittel et al., 2007) or competition indicators, such as the complexity of the canopy layer, the characteristics of neighboring trees and the species composition (Pretzsch and Rais, 2016). Alternatively, tree-specific variables, e.g. the morphologies of stems and crowns and the relationships between them, more explicitly reflect the individual responses of trees to an environment (Kuprevicius et al., 2013; Lindström, 1996; Moberg, 2006).

Integrating the mapping of wood properties into existing forest inventory regimes requires that the acquired remote sensing data capture tree-specific wood quality indicators, that is stem and crown descriptors across various stands. Dense airborne laser scanning (ALS) data has been shown effective at the delineation of individual tree crowns (Hyyppä and Inkinen, 1999; Lindberg and Holmgren, 2017; Næsset and Økland, 2002; Wang et al., 2016), and the estimation of various wood properties or their indicators (Fischer et al., 2018; Hilker et al., 2013; Luther et al., 2014; Maltamo et al., 2018). Previously, many of these indicators were challenging to measure in the field, however the recent emergence of terrestrial point cloud data from various sensors and platforms has enabled detailed structural measurements of standing timber (Liang et al., 2018a, 2018b; Liu et al., 2018). While operational applications, such as laser scanners integrated in harvesters, are still under development, terrestrial laser scanning (TLS) remains one of the most accurate technologies to acquire highly detailed three-dimensional (3-D) point clouds of individual trees in the forest environment (Dassot et al., 2011; Liang et al., 2016b; Maas et al., 2008; Newnham et al., 2015). The spatial range of TLS suits data acquisition on individual sample trees or plots, accompanied by geometric tree-modeling methods for the 3-D reconstruction of individual tree stems and branches (Bucksch and Lindenbergh, 2008; de Conto et al., 2017; Gorte and Pfeifer, 2004; Liang et al., 2012; Pyörälä et al., 2018c; Raumonen et al., 2013; Xia et al., 2015). The accuracies of various tree-specific wood quality indicators resolved from TLS point clouds was reported to be promising in previous studies (Barbeito et al., 2017; Höwler et al., 2017; Kankare et al., 2014; Murphy et al., 2010; Pyörälä et al., 2018a), as well as the wood and fiber properties predicted using TLS point cloud features at stand-level (Blanchette et al., 2015; Giroud et al., 2019).

There is an increasing consensus that future advances in high-resolution remote sensing technologies will come as a result of merging aerial and terrestrial sources to exploit their inherent strengths and reduce their potential weaknesses (Holopainen et al., 2014; Lindberg et al., 2012; Wang et al., 2019). The combining of airborne and terrestrial perspectives offers significant promise as complex tree-specific structural attributes can be measured with terrestrial sensors and extrapolated over larger areas using airborne and satellite data collection (Van Leeuwen et al., 2011). This requires that logical relationships should exist between terrestrially observable stem and branching properties and aviary observable crown characteristics.

However, studies that used a combination of ALS and TLS data to study tree-specific stem and crown descriptors are still few and several questions remain. In this study, our aim was to clarify the accuracy of predicting tree-specific wood quality indicators using a fusion of ALS and TLS, and to analyze the results with respect to the theoretical background of wood formation and forest management. To do so we derived estimates of the stem and crown dimensions that have been used as wood quality indicators in the previous literature, i.e., diameter at breast height (*DBH*), volume of the sawlog section (stem diameter > 15 cm) (V_{sawlog}), height of live crown base (H_{lc}), height of the lowest dead branch (H_{db}), and maximum branch diameter (*MBD*) using TLS point cloud based geometric tree models. We then modeled the extracted wood quality indicators with respect to features delineated from ALS point clouds that described the stand conditions, between-trees competition, and tree-specific characteristics.

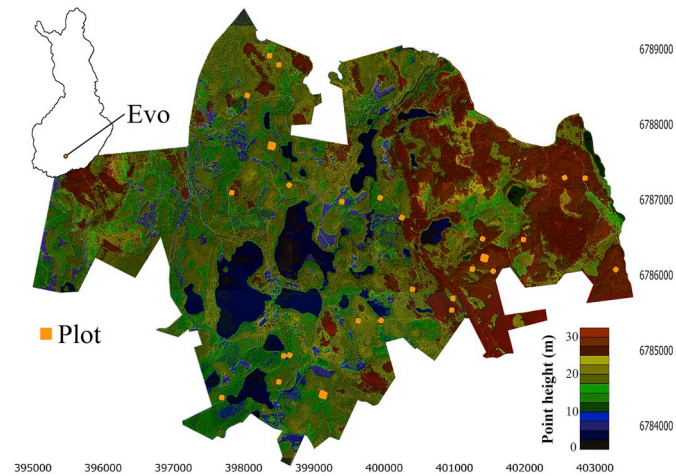

Fig. 1. Study area (Evo) and sample plot locations within the area. The area is illustrated by the airborne laser scanning (ALS) point clouds used to aid stand selection; pixel colors indicate the mean height of ALS points above ground. The coordinates are given in meters according to the EUREF-FIN coordinate system. (For interpretation of the references to color in this figure legend, the reader is referred to the Web version of this article.)

2. Materials

2.1. Study design

The study area comprised ca. 2000 ha of southern boreal forests in the Evo locality, southern Finland (Fig. 1). The average stand size is approximately 2 ha. We focused on 27 even-aged, managed homogeneous Scots pine dominated stands at young, developed and mature development stages, as indicated by the basal area (*G*), basal-area weighted mean *DBH* (*DG*), and the mean tree height (*H*) of the 100 largest trees in *DBH* per hectare, i.e., dominant height (H_{dom}) (Table 1, Fig. 2). Stand selection was aided with grid-based wall-to-wall ALS point height information over the study area to ensure we captured a representative spectrum of stand conditions over the area (Fig. 1). We established 24 sample plots of 32 × 32 m, one per stand, across the range of variation. In addition, in the remaining 3 stands, which fully represented the transition from young to mature forest within similar stand conditions, we placed 4 plots per stand for the purpose of validating the representativeness of our sampling and to analyze the performance of our methods. The total number of sample plots was thus 36.

2.2. Terrestrial laser scanning data acquisition

TLS data were acquired from May to July 2014 using either of the following two phase-shift scanners: Leica HDS6100 (Leica Geosystems

Table 1
The descriptive statistics of study material. G is the basal area, H_{dom} the dominant height, and DG the basal-area weighted mean diameter of trees. The numbers indicate average (+/− standard deviation) within the category, calculated from the sample plot data.

	Modelling data (24 stands)					Validation data (3 stands)				
Class	Plots (n)	G (m^2/ha)	DG (cm)	H_{dom} (m)	Stems (N/ha)	Plots (n)	G (m^2/ha)	DG (cm)	H_{dom} (m)	Stems (N/ha)
Young	8	20.09 ± 8.04	17.52 ± 1.81	165.93 ± 29.68	1179.20 ± 414.58	4	16.49 ± 1.21	19.42 ± 0.89	174.58 ± 4.01	637.21 ± 116.75
Developed	10	23.21 ± 4.96	21.62 ± 0.65	207.71 ± 18.06	845.70 ± 287.50	4	20.24 ± 2.54	25.65 ± 1.75	212.33 ± 4.57	490.72 ± 68.77
Mature	6	24.44 ± 2.93	26.46 ± 2.90	236.22 ± 25.13	618.49 ± 189.23	4	23.36 ± 0.89	27.92 ± 2.78	237.68 ± 2.00	449.22 ± 46.49

AG, Heerbrugg, Switzerland) and Faro Focus^{3D} X 330 (Faro Technologies Inc., FL, USA). The HDS6100 uses a wavelength of 650–690 nm and the Focus^{3D} X 330 a wavelength of 1550 nm. Both scanners have a 3 mm beam diameter at exit, and we used scanning settings that resulted in a point spacing of 6.3 mm at a distance of 10 m from the scanning location (in our data, ~10000 points per square meter). We scanned each plot at five locations: at plot center and at the northeast, southeast, southwest, and northwest plot corners, based on compass directions.

Six target spheres with a diameter of 198 mm were used as reference targets to enable data registration. We placed one sphere directly to magnetic north from the center scan location and distributed the rest of the spheres evenly around the plot, ensuring that all six spheres were visible to the center scan and at least three to each of the other scans.

2.3. GNSS positioning and tree mapping

We recorded the global coordinates of the TLS target spheres in the field using two reference points in open areas near the plot (e.g., road, lakeshore, clearing) using a Trimble R8 GNSS receiver (Trimble Inc., CA, USA) with real-time kinematic signal correction. We used a Trimble 5602 DR200 + total station to establish a survey point inside each plot by measuring the distances and angles to the reference points and then measured the sphere locations from the survey point using the total station. We calculated plot corner coordinates using the aforementioned sphere coordinates. Given the difference between magnetic and true north, the orientation of a plot in the field had to be solved using the coordinates of the north sphere and center scan (EUREF-FIN). After that, we calculated the plot corners, accordingly, detected all visible trees within the plot borders in the TLS point cloud, and created a preliminary tree map for a field crew.

2.4. Field data acquisition

The field crew acquired tree-specific field data from the sample plots between May and August 2014. The measurers used the TLS-based tree maps to identify plot borders and to locate each tree with DBH exceeding 5 cm within the plot. Omitted trees were added to the map. For each tree, the field crew identified their species and measured H and DBH using a digital Vertex III hypsometer (Haglöf Sweden AB, Långsele, Sweden) and calipers, respectively. For Scots pine trees, also H_{db} and H_{lc} were measured using the Vertex. All Vertex measurements equaled an average of three repetitions. DBH was defined as an average of two perpendicular measurements at a height of 1.3 m above the root collar. Using the field measurements, we calculated tree-specific V_{sawlog} and MBD by applying previously presented species-specific equations for the vertical variation of stem and branch diameters in Scots pine in Finland (Laasasenaho, 1982; Mäkinen and Colin, 1998). The stem taper equation used DBH and H (Appendix I), whereas the branch diameter equations used DBH, relative crown length (H-H_{lc}/H), and the estimated number of whorls from the stem apex as explanatory variables (Appendix II).

2.5. Airborne laser scanning data acquisition

ALS data over the entire study area were acquired in September 2014. The scanner was a Leica ALS70-HA. The data were collected from an altitude of 900 m above sea level at a speed of 150 knots with a pulse rate of 240 kHz, and the resulting data had an average pulse density of 6 pulses per m^2 with a footprint of 13.5 cm. The system recorded a maximum of 5 echoes per pulse.

3. Methods

3.1. Terrestrial laser scanning preprocessing

TLS point clouds from the five scanning locations were co-registered into the EUREF-FIN coordinate system using the sphere locations measured in the field. Simultaneously, the stochastic noise (stray points and dark points) was filtered from the TLS point clouds based on grid-based analyses of point intensity values and point densities by the built-in algorithms in the software used—Faro Scene 5.2 and Leica Z + FLaserControl 8.6, respectively.

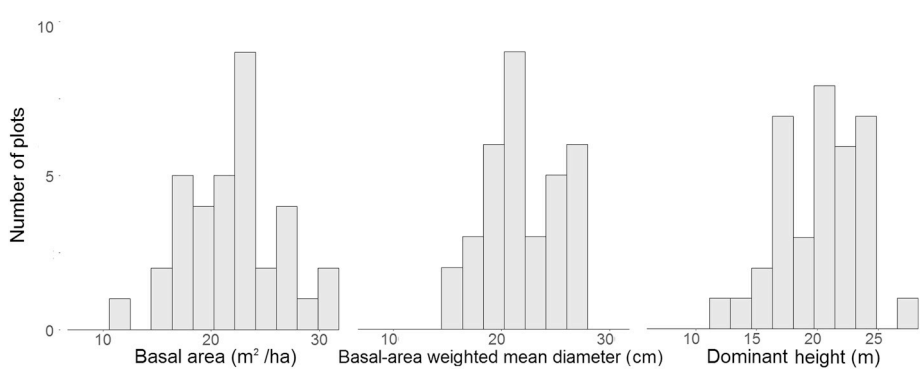

Fig. 2. Distribution of basal area, basal-area weighted mean diameter, and dominant height of the sample plots (N = 36).

3.2. Sample tree selection and extraction from terrestrial laser scanning point clouds

We selected a systematic sample of trees from the TLS point clouds of each plot with the aim of representing the original diameter distribution. The sampling was based on the field-verified tree map. A number of Scots pine trees (n) equaling 10% of the total number of Scots pine trees in each plot was sampled by ordering the trees according to their *DBH*, dividing the ordered tree list into n sections each including an equal number of trees, and choosing a random tree from each section.

The selected sample trees were extracted from the TLS point clouds using a canopy segmentation method. To speed up the process, we thinned TLS multi-scan point clouds temporarily to a density where points were averaged into a single point in a 50 cm 3-D neighborhood. We then classified ground points using an iterative triangulation algorithm and fitted a digital terrain model (DTM) with a 50 × 50 cm resolution to the ground points (Axelsson, 2000) with TerraScan software (Terrasolid oy, Helsinki, Finland). A digital surface model (DSM) with an identical resolution was subsequently derived from the highest returns, and a normalized canopy height model (CHM) was generated by subtracting the DTM from the DSM (Fig. 3d). We segmented the CHM into individual tree crowns using a local maxima based iterative area-growing algorithm (Dalponte and Coomes, 2016) using R-package lidR 2.0.0 (Roussel and Auty, 2019) (Fig. 3e).

We extracted points from TLS point clouds in original point density within the segment that had the smallest Euclidean distance to each sampled tree according to the tree location in the field data. We examined the contents of extracted trees within the segments manually. Failed segmentation occurred due to i) heavy occlusion making identification of a tree stem and/or individual branches difficult, ii) the tree being dead, or iii) other than the dominant species, the tree was rejected from the final sample. The segments were not manually modified, that is, no removal of ground, understory, surrounding tree canopies, or other cleaning of the point cloud was carried out. The final sample included 268 trees for stem modeling, out of which 242 trees were also suitable for branch modeling.

3.3. Geometric tree modeling and the estimation of wood quality indicators

The geometric tree modeling followed the principles described in Liang et al. (2012) and Pyörälä et al. (2018c). In summary, we downsampled the points into 0.5 × 0.5 × 0.5 cm voxels and carried out principal component analysis (PCA) for 3-D points in the neighborhood of the 100 nearest voxels. We classified the points based on their orientation as indicated by eigenvectors, and flatness represented by eigenvalues (Liang et al. (2012). Flat, vertical objects were classified as belonging to a tree stem, and other flat objects were classified as belonging to branches (Fig. 3c). The rest of the points were filtered out as stochastic noise. We modeled the stem by fitting consecutive cylinders to stem points from tree bottom to top and generated a continuous taper function using cubic spline smoothing on the estimated stem diameters with respect to height (Fig. 4), with the smoothing parameter set to 0.4 (Saarinen et al., 2017). For branch detection, the stem model was split into vertical segments 15 cm in height in 5-cm intervals, that is, 15-cm consecutive segments with a 10-cm vertical overlap (Pyörälä et al., 2018c). The distribution of branch points in each vertical segment as a function of degrees around the stem was smoothed by a convolution with Gaussian window function. Branches were identified in the smoothed distribution using a continuous wavelet transform peak-detection method (Du et al., 2006). The detected branch points were projected onto a horizontal plane using their eigenvector direction and modeled as a circle utilizing the random sample consensus (RANSAC) algorithm (Fischler and Bolles, 1981): the z-coordinate and diameter of the fitted circle were considered to be the branch height (b_h) and branch diameter b_d, respectively (Fig. 3c). Tree-specific b_d observations were smoothed with respect to b_h using a cubic spline with smoothing parameter 0.7 (Fig. 4).

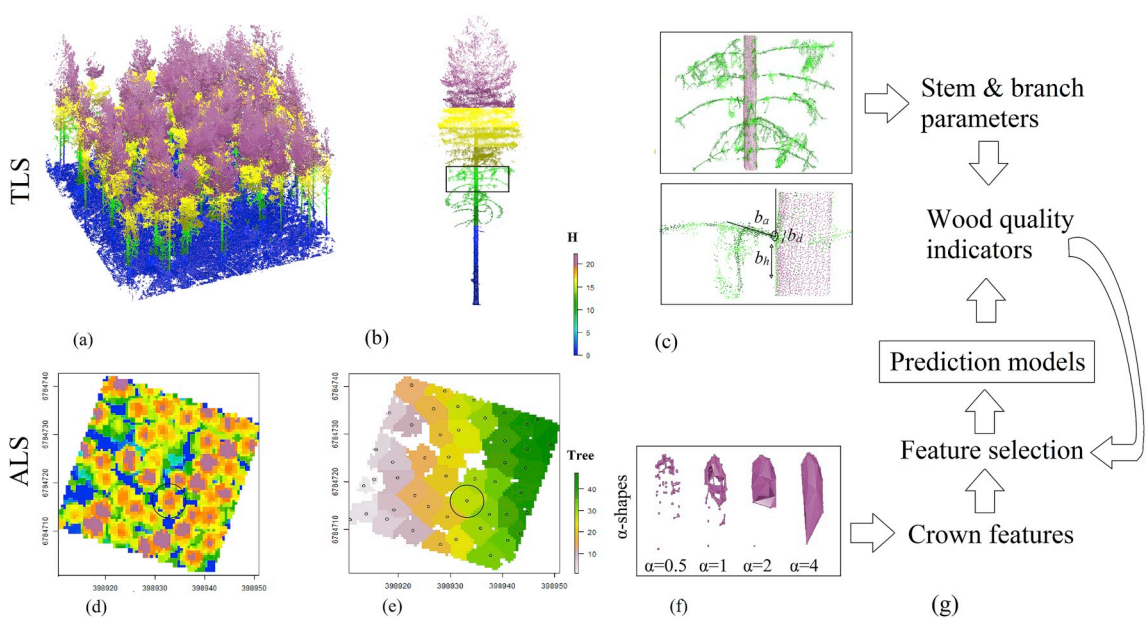

Fig. 3. Material and methodologies used in this study. (a) Example of terrestrial laser scanning (TLS) point cloud from a sample plot. Colors indicate point height (H) above ground. (b) Example of TLS sample tree extracted from the sample plot. (c) 1 m vertical section of the example sample tree with points classified as crown points (green) and trunk points (purple), as well as the parameters extracted for each detected branch: b_α = branch insertion angle, b_d = branch diameter, and b_h = branch height from ground. (d) Airborne laser scanning (ALS) canopy height model (CHM) of the sample plot. The x- and y-coordinates (m) refer to EUREF-FIN coordinate system. (e) Results of tree detection and tree crown segmentation from the CHM. Tree segment matched to the TLS sample tree in b) is circled. (f) As an example of ALS feature extraction, α-shapes fitted to the example tree segment with α = 0.5, 1, 2, and 4, from left to right. (g) Modeling scheme. Wood quality indicators were inferred from the stem and branch parameters of TLS sample trees. Stand and tree-specific ALS crown features that explained the most variability of the wood quality indicators were selected using regression trees, and Random Forest was used to build the respective prediction models. (For interpretation of the references to color in this figure legend, the reader is referred to the Web version of this article.)

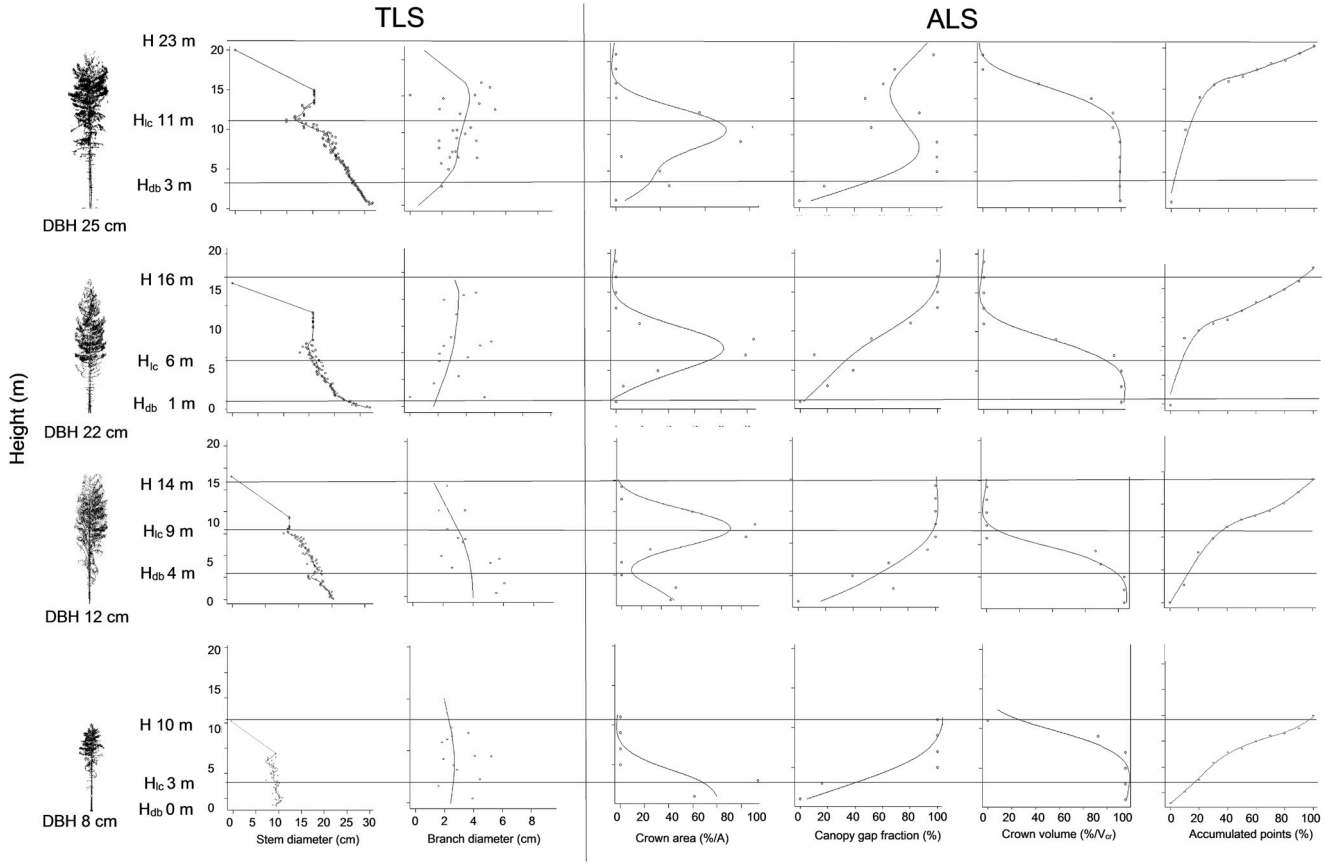

Fig. 4. Height dependent relationships between terrestrial laser scanning stem and branch diameters and tree-specific airborne laser scanning features in four example trees at different development stages, as indicated by the diameter at breast height (*DBH*). The vertical curves depict the cubic spline smoothing of each variable with respect to height. Horizontal lines indicate height of the lowest dead branch (H_{db}), height of the live crown base (H_{lc}), and tree height (H) measured in the field.

We estimated the following proxies of wood quality indicators tree-specifically based on an analysis of the smoothed functions of the taper curve and vertical distribution of branch diameters with respect to the field reference data (Fig. 4):

- Stem diameter at 1.3 m height above ground: DBH_{TLS}
- Volume of stem with diameter > 15 cm: $V_{sawlogTLS}$
- The b_h at maximum b_d: H_{lcTLS} (i.e. we assume maximum b_d is found at H_{lc})
- Minimum b_h: H_{dbTLS}
- Maximum b_d: MBD_{TLS}

3.4. Airborne laser scanning feature extraction

We clipped the full ALS data using the plot corner coordinates. We delineated individual tree crowns from the data using an identical CHM segmentation algorithm as with the TLS point clouds, (Dalponte and Coomes, 2016), and calculated several geometric and point-based features for each tree segment, each associated with one of three groups, namely tree, stand, and competition descriptors (Table 2). The TLS sample trees were each matched to a corresponding ALS segment and field-measured tree based on the smallest horizontal distance.

The tree-specific features included the segment area (A_{seg}), crown volume V_{cr}, point height percentiles (H_0, H_{10}, … H_{100}) as well as the vertical crown gap fraction, crown area, and subtractive crown volume profiles extracted using R-packages lidR and alphashape3d 1.3 (Lafarge and Pateiro-Lopez, 2017) (Supplementary Material 1).

The crown volumes were produced using alpha shapes (α-shapes: convex hull weighted by α to remove triangle simplices longer than α^2) (Edelsbrunner and Mücke, 1994) (Fig. 3c). V_{cr} was calculated using α = 999. The point height percentiles refer to the heights where the given percentage of points have accumulated. The vertical crown gap fraction and crown area profile values refer to the probability of a gap and the area occupied by points, respectively, within each consecutive 2 m high section from ground level to the height of a tree. The subtractive crown volume profile gives the volume of the points above fixed heights with 2 m vertical intervals. We used alternate α-values of 0.5, 1, 2, and 4 (Fig. 3c). Cubic spline smoothing of the obtained height dependent crown profiles was used to estimate the logical proxies of H_{lc}, i.e., heights of the maximum crown area (H_{MAX_A}) and maximum α-shape volume ($H_{MAX_V_\ \alpha=0.5,1,2,4}$) (Fig. 4). We reduced the dimensionality of these vertical profiles into the first principal component (PC) using PCA. The stand descriptors included the number of trees and crown area per hectare and mean and maximum H_{100} and A_{seg} in each plot. The competition variables included tree-specific mean distances to the three nearest trees, and H_{100} and A_{ses} values relative to the plot-specific mean and maximum H_{100} and A_{seg} values, as well as the mean of the nearest three trees.

3.5. Airborne laser scanning feature selection and Random Forest predictions

Pearson's correlation coefficients (r) between the wood quality indicators studied and the ALS features were inspected to screen the linear dependencies between them. However, due to the inevitably complex (i.e., nonlinear) interactions between the wood quality indicators and various tree, stand, and competition factors, we applied regression trees (Breiman et al., 1984) to select the sets of ALS features

Table 2
List of airborne laser scanning features used in this study and their group associations and abbreviations.

Group	Feature	Abbreviation	Unit
Tree descriptors			
	Segment area	A_{seg}	m^2
	Full crown volume with α = 999	V_{cr}	m^3
	Point height percentiles 0–100%, by 10%	H_0, H_{10}, …, H_{100}	m
	First principal component of point height percentile profile	H_{PC1}	m
	Height of the maximum height percentile increment	H_{MAX_Incr}	m
	First principal component of vertical canopy gap fraction profile	gf_{PC1}	*
	First principal component of vertical crown area profile	A_{PC1}	*
	Height of the maximum crown area	H_{MAX_A}	m
	First principal component of subtractive crown volume profiles with α = 0.5, 1, 2, and 4	V_{PC1_α}	*
	Base height of the maximum crown volume with α = 0.5, 1, 2, and 4	$H_{MAX_V_\alpha}$	m
Stand descriptors			
	Plot mean tree height	H_{mean}	m
	Plot maximum tree height	$H_{\max}$	m
	Number of trees	N_{trees}	N/ha
	Plot canopy coverage	A_{total}	m^2
	Plot mean segment area	A_{mean}	m^2
	Plot maximum segment area	$A_{\max}$	m^2
Competition descriptors			
	Mean horizontal distance to three nearest trees	*Dist*	m
	Relative height to plot mean	$H_{RelMean}$	%/100
	Relative height to plot maximum	H_{RelMax}	%/100
	Relative height to the means of three nearest trees	H_{RelNN}	%/100
	Relative segment area to plot mean	$A_{RelMean}$	%/100
	Relative segment area to the means of three nearest trees	A_{RelNN}	%/100
	*component score		

that could most comprehensively predict the response variables. We built regression trees for each wood quality indicator studied and selected the node features as explanatory variables using R-package rpart 4.1 (Therneau and Atkinson, 2018) (Supplementary Material 2).

Random forest's (RF) (Breiman, 2001) were then used to correct possible over-fitting of the regression trees to our sample tree data with iterative resampling (or bootstrapping) of the data (White et al., 2017), with R-package randomForest 4.6 (Liaw and Wiener, 2002) (Supplementary Material 2). RF generated separate forests of 2000 regression trees for each TLS attribute and randomly selected two thirds of the data for training in each tree. RF permuted between two features randomly picked from the pre-selected features in each node. Simultaneously to the bootstrapping, RF evaluated the prediction accuracy against one third of the sample tree data (out-of-the-bag, OOB, sample). We reported the importance of the explanatory features in terms of the proportional increment of the mean squared error (MSE-INC) of the OOB sample for each regression tree before and after permuting the predictor variable, and the total decrease in the residual sum of squares (RSS-DEC) in OOB from the splitting of the variable. The final prediction output was a regression tree averaged over all repeated bootstraps.

3.6. Evaluation of the methods

First, we evaluated the accuracy and performance of our measurement and modeling methods: i) We compared the tree-specific values derived from TLS tree models with those based on the field measurements, i.e., we assessed the accuracy of the observed (subscript TLS) values. ii) We evaluated the accuracy of the predicted values (DBH_{RF}, $V_{sawlogRF}$, H_{lcRF}, H_{dbRF}, MBD_{RF}) in terms of R^2 and root mean squared error by comparing the predicted (subscript RF) and TLS-derived values in sample trees. iii) We used the RF models to predict wood quality indicators over all delineated tree segments within our sample plots and compared resulting probability density functions with those of the TLS sample tree measurements, as well as the field-based observations of all trees in the sample plots.

Then, we demonstrated the performance of our methods in describing the variability of wood quality indicators between stands. We extrapolated the wood quality indicator predictions over three of our study stands (Fig. 1) that represented different developmental stages, namely a transition of managed Scots pine stands from young to mature forest (as indicated by H_{dom}, G, and DG) and had four sample plots each. We processed the stand-specific ALS point clouds similarly to those in the plot-level data and used our RF models to predict tree-specific wood quality indicators with respect to the crown features of delineated trees. We standardized the wood quality indicator values, that is, calculated the z-scores of the values with respect to the mean and standard deviation of predicted values over all trees in all stands:

$$z_i = \frac{y_i - \bar{y}}{\frac{1}{n}\sum_{i=1}^{n}(y_i - \bar{y})} \tag{1}$$

where z_i is the z-score and y_i the predicted value of wood quality indicator studied in tree i, respectively, and $\bar{y}$ is the mean over all n observations. Then, we calculated Euclidean distances between all individual trees based on the z-scores of each indicator separately, as well as all together, and used hierarchical clustering to group trees into clusters of similar individuals (Ward, 1963) (Supplementary Material 2). We analyzed the clustering of the trees with respect to the stand and plot associated with each tree: i) to assess the representativeness of our sampling and modeling scheme in the studied stands and ii) to identify variabilities of wood quality characterized by the wood quality indicators.

4. Results

4.1. Feature selection

We observed the highest linear correlations between DBH_{TLS}, $V_{sawlogTLS}$, and H_{lcTLS}, and the ALS point height features (percentiles H_{40}…H_{100}, H_{mean}, $H_{\max}$, and H_{RelMax}), the first PCs of accumulated points, the canopy gap fraction, and the subtractive crown volumes (Table 3). No strong correlations were observed between H_{dbTLS} and MBD_{TLS} and any ALS feature (Table 3). Despite the close correspondence between H_{MAX_A} and $H_{MAX_V_\alpha=0.5,1,2,4}$ with H_{lc} in the empirical data (Fig. 4), their correlations remained low (Table 3).

Table 3
Pearson's correlation coefficients between the wood quality indicators and airborne laser scanning features. See Table 2 for abbreviations.

		DBH_{TLS}	$V_{sawlogTLS}$	H_{lcTLS}	H_{dbTLS}	MBD_{TLS}
Wood quality indicators	DBH_{TLS}	1.00	0.93	0.39	0.17	0.20
	$V_{sawlogTLS}$	0.93	1.00	0.43	0.19	0.16
	H_{lcTLS}	0.39	0.43	1.00	0.40	0.06
	H_{dbTLS}	0.17	0.19	0.40	1.00	−0.12
	MBD_{TLS}	0.20	0.16	0.06	−0.12	1.00
Tree descriptors	A_{seg}	0.22	0.22	0.23	−0.04	0.16
	V_{cr}	0.31	0.37	0.31	0.10	0.07
	H_0	−0.02	−0.03	0.06	−0.07	0.03
	H_{10}	0.30	0.33	0.21	0.01	0.18
	H_{20}	0.38	0.40	0.25	0.13	0.15
	H_{30}	0.44	0.45	0.27	0.17	0.15
	H_{40}	0.54	0.54	0.42	0.29	0.13
	H_{50}	0.63	0.63	0.52	0.36	0.12
	H_{60}	0.65	0.66	0.55	0.37	0.14
	H_{70}	0.67	0.68	0.55	0.35	0.14
	H_{80}	0.70	0.70	0.57	0.35	0.14
	H_{90}	0.70	0.71	0.57	0.35	0.14
	H_{100}	0.71	0.72	0.55	0.32	0.13
	H_{PC1}	−0.66	−0.67	−0.55	−0.34	−0.16
	$H_{MAX\ Incr}$	0.10	0.07	0.22	0.16	−0.10
	gf_{PC1}	−0.53	−0.56	−0.38	−0.31	−0.02
	A_{PC1}	0.45	0.49	0.32	0.22	0.05
	$H_{MAX\ A}$	0.39	0.41	0.26	0.22	0.12
	$V_{PC1\ 0.5}$	0.23	0.28	0.21	0.10	−0.04
	$V_{PC1\ 1}$	−0.33	−0.37	0.22	0.08	0.04
	$V_{PC1\ 2}$	−0.45	−0.48	−0.30	−0.10	−0.18
	$V_{PC1\ 4}$	−0.47	−0.50	−0.32	−0.13	−0.18
	$H_{MAX\ V\ 0.5}$	0.21	0.23	0.13	−0.01	0.13
	$H_{MAX\ V\ 1}$	0.30	0.33	0.19	0.02	0.15
	$H_{MAX\ V\ 2}$	0.28	0.28	0.22	0.03	0.10
	$H_{MAX\ V\ 4}$	0.25	0.22	0.23	0.09	0.06
Stand descriptors	H_{mean}	0.63	0.67	0.63	0.41	0.08
	H_{max}	0.61	0.66	0.60	0.43	0.07
	N_{trees}	−0.25	−0.27	−0.07	0.00	−0.38
	A_{total}	0.14	0.20	0.23	0.18	−0.21
	A_{mean}	0.28	0.30	0.27	0.13	0.06
	A_{max}	0.17	0.18	0.26	0.17	−0.11
Competition descriptors	$Dist$	0.28	0.30	0.11	−0.06	0.19
	$H_{RelMean}$	0.31	0.25	−0.05	−0.06	0.09
	H_{RelMax}	0.49	0.44	0.24	0.07	0.14
	H_{RelNN}	0.22	0.17	0.06	0.07	0.06
	$A_{RelMean}$	0.07	0.04	0.08	−0.12	0.06
	A_{RelNN}	−0.05	−0.06	−0.01	−0.06	0.02

According to the regression tree based feature selection, point height features (e.g., H_{100}, H_{80}, H_{70}) explained most of the variance in stem size variables (DBH_{TLS} and $V_{sawlogTLS}$)—ALS height percentiles were the most abundant splitting nodes that could divide the data into four more or less equally sized bins (Fig. 5). The importance of calculations based on RF (Fig. 6) supported the significance of the linear relationship of these features with stem size that was observed in the correlation matrix too (Table 3). Some additional dependency of the stem size on stand and competition factors (N_{trees} and H_{RelMax}) resulted in small additional splits to regression trees (Fig. 5) that were able to improve MSE-INC and RSS-DEC if less than the tree descriptors (Fig. 6).

H_{lcTLS} was mostly explained by the stand descriptors (point height features H_{mean} and H_{max}) and tree descriptors (height percentiles H_{100}, H_{60}, and crown volume V_{cr}) (Fig. 5). Stand-specific H_{mean} divided H_{lcTLS} observations roughly into two (Fig. 5) and improved MSE-INC by almost 50% (Fig. 6). Additional tree and competition descriptors explained some of the remaining variances (Figs. 5 and 6).

H_{dbTLS} and MBD_{TLS} were poorly associated with ALS features (Fig. 5). 40% of H_{dbTLS} was associated with a single end node with predicted value 3.2 m, just two splitting nodes away ($H_{max} < 19$ m and $H_{90} < 17$ m) from the sample mean, 4.9 m (Fig. 5). For MBD_{TLS}, the competition indicator H_{RelMax} and tree descriptor, height percentile H_{50} split the data into three bins of 51%, 31%, and 18% of observations with means of 3.3 cm, 3.7 cm, and 3.9 cm, respectively (Fig. 5).

4.2. Model predictions

TLS-derived wood quality indicators for the stem variables (DBH_{TLS}, $V_{sawlogTLS}$) concurred with their correspondences measured in the field ($R^2 > 0.8$) (Fig. 7). H_{lcTLS} had R^2 of 0.20, while H_{dbTLS} and MBD_{TLS} had R^2s < 0.1, when compared to their field-measured values (Fig. 7).

Based on the feature selection, wood quality indicator predictions of DBH_{RF}, $V_{sawlogRF}$, and H_{lcRF} had R^2 values of 0.51, 0.50, and 0.40, respectively, while H_{dbRF} ($R^2 = 0.25$) and MBD_{RF} ($R^2 = 0.03$) were more challenging to model using the ALS features (Fig. 7). Under- and overestimates of the lower and upper extremes, respectively, were present in all models (Fig. 7).

The probability density functions of DBH_{TLS}, H_{lcTLS}, H_{dbTLS}, and $MDBTLS$ of the sample trees represented those of corresponding field-measured variables in the sample plot data (Fig. 7). However, DBH_{RF} predicted over the sample plots using ALS features resulted in a notably narrower variance around the mean when compared with the original function (Fig. 7). $V_{sawlogTLS}$ and $V_{sawlogRF}$ had similar probability density functions to each other but were not able to capture the share of stems smaller than the sawlog size (diameter < 15 cm) that were present in the field data (Fig. 7). H_{lcRF} and H_{dbRF} represented well those of corresponding field-measured variables in the sample plot data (Fig. 7). MBD_{RF} did not comprehensively represent the variance observed in both field and sample tree TLS data, but the mean value was unbiased (Fig. 7).

4.3. Variability of wood quality indicators

The tree-specific mean z-scores of predicted wood quality indicators varied more between stands than between plots of the same stand (Fig. 8a). When the z-scores of *DBH* and V_{sawlog} were considered, the data were hierachically clustered into two groups (Fig. 8c). Namely, the stand at the earliest development stage examined differed more from the two more mature stands than the latter differed from each other. However, H_{lc} made it possible to also distinguish between the mature stands: H_{lc} z-scores exhibited notable differences between all three stands. Moreover, the youngest stand had two distinct clusters of trees with notably different H_{lc} z-scores. H_{lc} thus clustered the trees into four different groups (Fig. 8). H_{db} behaved synchronously to the increasing tree size, i.e. showed clear distinctions between the youngest and the more mature stands, but *MBD* was not useful in distinguishing between the stands.

5. Discussion

Our results showed that while it was challenging to associate wood quality indicators related to branching in the lower canopy (H_{db}, *MBD*) with ALS features, wood quality indicators describing dimensions of stem and live crown (*DBH*, V_{sawlog}, H_{lc}) were predictable from ALS point clouds (Fig. 7). The predicted wood quality indicators enabled logical distinctions between forest stands. For example, while stem sizes between two mature stands were very similar, the crown sizes still differed (Fig. 8). The results likely reflect the fact that for Scots pine, the canopy closure regulates the crown length in mature stands and decelerates the radial growth in stems below H_{lc}, resulting in the increase of stem taper above H_{lc} (Fig. 4). The interpretation was supported by the visually observed canopy closure from the youngest to the more mature stands (Fig. 8a). Potentially, size-mediated wood formation processes, e.g., the formation of knots and juvenile wood, could be modeled from the combination of stem and crown size, with implications for various wood properties, e.g. wood density. In other words, the

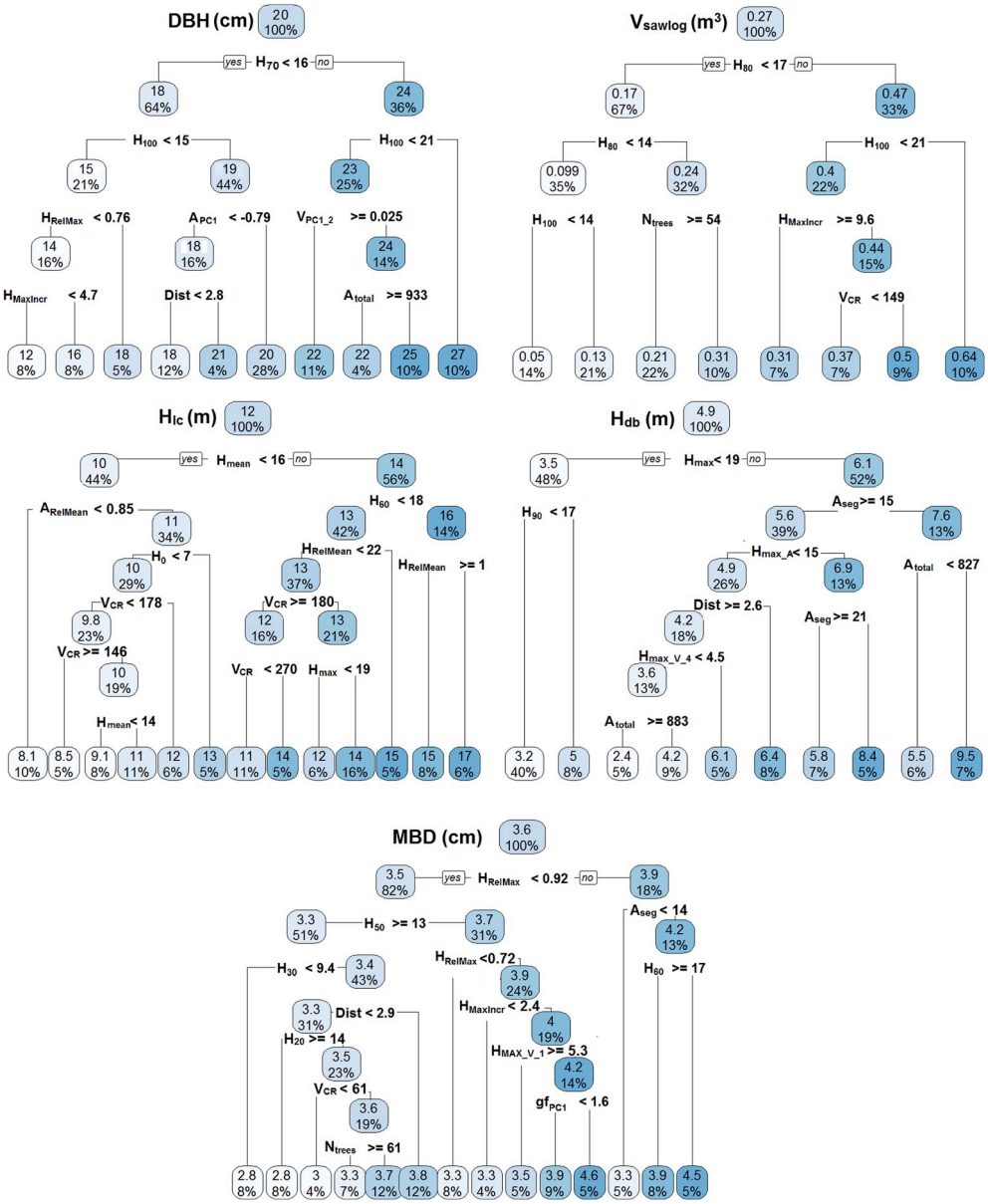

Fig. 5. Results of the feature selection. Regression trees used in airborne laser scanning feature selection for each wood quality indicator (diameter at breast height *DBH*, sawlog volume V_{sawlog}, height of the live crown base H_{lc}, height of the lowest dead branch H_{db}, and maximum branch diameter *MBD*). Each node gives the mean value (also indicated by the node shading—the darker the shade, the larger the value) and the percentage of observations associated with that node. Splits give the splitting variables and the respective decision criteria. See Table 2 for ALS feature abbreviations and units.

inclusion of H_{lc} in remote sensing - based inventory variables, in addition to stem size variables, could be used to compare stands at similar development stage. Ultimately, the information could be used to more precisely tune forest management options to improve the carbon sequestration in forests, and to target the harvesting operations according to wood quality.

We showed that obtaining detailed ALS and TLS data on stem and crown dimensions from a relatively small sample of trees can be used to build reliable models to predict tree-specific stem and crown size variables over forest stands (Fig. 8). Previously, Hilker et al. (2010) and Hilker et al. (2012) compared TLS and ALS in deriving stand structure parameters and concluded that the characteristics of the upper canopy described by ALS and the structure of the lower canopy described by TLS both correlated well with *G*, implying that the relationship of wood quality to stand conditions and competition was captured with either method. Our study confirmed that logical relationships exist between the terrestrially and aerially observable canopy characteristics also tree-specifically. Further work is required to expand the tree-specific relationships from stand level to landscapes or larger regions.

Our sampling scheme aimed to preserve the original diameter distribution of the plots. The selected sample trees mostly represented the shape of the wood quality indicator probability density functions within our sample plots, although the proportion of small trees (diameter < 15 cm) was underrepresented in our sample (Fig. 7). Based on the further analysis of subsamples from three stands, the one-plot sample likely covered stand-specific variability of wood quality indicators (Fig. 8). Our sampling was based on conventional field data covering all trees in a plot. However, it could also be possible to utilize TLS-based stem maps, as demonstrated by Vastaranta et al. (2014) and Saarinen et al. (2014). TLS can record up to 90–100% of trees at breast height with a scanning setup similar to ours in conditions favorable to TLS, such as intensively managed Scots pine stands like those used in our study (Table 1) (Liang et al., 2018a).

Our results confirm previous studies in that TLS can provide

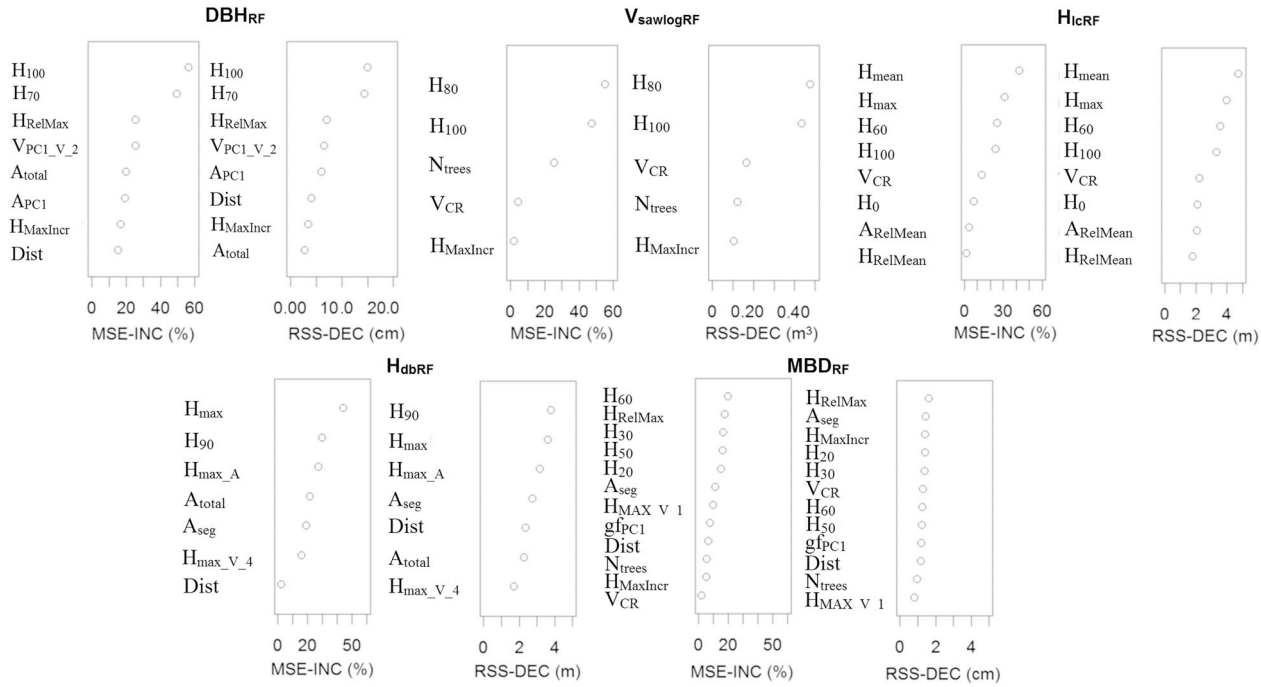

Fig. 6. Importance of airborne laser scanning (ALS) features in Random Forest bootstrapping of the wood quality indicators (diameter at breast height *DBH*, sawlog volume V_{sawlog}, height of the live crown base H_{lc}, height of the lowest dead branch H_{db}, and maximum branch diameter *MBD*). MSE-INC is the proportional increment of the mean squared error, and RSS-DEC the total decrease of the residual sum of squares. See Table 2 for ALS feature abbreviations and units.

accurate estimates of stem dimensions and volume (Liang et al., 2014; Saarinen et al., 2017), while the crown and branching parameters are more difficult to obtain reliably (Pyörälä et al., 2018b; Wilkes et al., 2017). Successful tree extraction plays a role in the accuracy of the stem and branching attributes retrieved from TLS point clouds. The extraction in this study used two-dimensional segmentation of tree crowns and manual verification of acceptable extraction results. Previous literature has presented several automated tree extraction and segmentation methods that could also be used to separate trees (Burt et al., 2018; Raumonen et al., 2015; Xia et al., 2015; Zhong et al., 2017). The segmentation of fused ALS and TLS data was specifically studied in Paris et al. (2017). In addition to methodologies, successful extraction and tree modeling is highly dependent on the density of the point cloud. Based on visual inspections of our data, the TLS point cloud density and distances between the scan locations in this study were not optimal for retrieval of branching structures for all trees, which is in line with previous literature (Wilkes et al., 2017).

Our results showed that wood quality indicators describing the stem and crown size were predictable from crown features extracted from ALS point clouds, which concurred with the major body of literature (Hilker et al., 2012; Lindberg et al., 2012; Maltamo et al., 2009, 2018). Common bottlenecks associated with ALS predictions are the challenges in species recognition and retrieving data from lower canopy layers (Chasmer et al., 2006; Korpela et al., 2010). In our study, species-specific differences in wood quality indicators were not considered, as the study focused on homogeneous Scots pine stands. Ideally, species recognition could be based on TLS tree-model phenology (Åkerblom et al., 2017), coincident with the estimation of wood quality indicators. The retrieval of data from lower canopy layers might be improved with high-resolution ALS data and, e.g. single-photon technology (Swatantran et al., 2016). Moreover, segmentation algorithms better suited to multilayered canopies are constantly developing (Aubry-Kientz et al., 2019; Hancock et al., 2017; Wang et al., 2016). These developments are especially crucial for such methods as presented in this study to be applicable for more complex forest structures including mixed, uneven-aged or unmanaged forests.

In previous literature, the mean values of several wood and fiber properties (e.g., wood density and microfibril angle) were modeled from stand-specific canopy structure and competition indicators retrieved from TLS (Blanchette et al., 2015; Giroud et al., 2019) and ALS data (Fischer et al., 2018; Hilker et al., 2013; Luther et al., 2014). These studies highlighted the influence of stand conditions and competition on wood formation. However, the direct links between wood properties and stand-level features were found to be inconsistent and not transferable between various stand conditions, which was likely due to the lack of explanatory variables to account for the tree-specific vertical and radial gradients of the wood properties. Indeed, the tree-specific stem and crown size variables that were found to be predictable from the fusion of TLS and ALS data in this study are important indicators of several wood properties that are dependent on tree age or size. Most prominently, crown length and vigor have known implications for the knottiness and juvenile wood content in the stem base (Kuprevicius et al., 2013; Mansfield et al., 2007). Therefore, the stem and crown size variables predictable from the combination of TLS and ALS data could be used to indicate the radial and vertical development of size-dependent wood properties.

For example, the vertical trends of branch (and knot) insertion angles and diameters can be modeled using common stand and tree descriptors (Björklund, 1997; Groot and Schneider, 2011; Maguire et al., 1999; Mäkinen and Colin, 1998; Moberg, 2006). *MBD* in this study was derived from field-measured variables using empirical models with parameter and error coefficients fitted to another data set (Mäkinen and Colin, 1998). Despite the bias of tree-specific estimates, the density distributions between *MBD* in full sample plot data and MBD_{TLS} in the sample tree data were unexpectedly similar (Fig. 7). Therefore, it should be tested whether *MBD* (and other branch diameters) could be predicted using the more readily predictable tree descriptors, e.g., *H*, *DBH*, and H_{lc}, with the parameters of the branch diameter equation calibrated using the branch diameters measured from the TLS point clouds—instead of direct predictions of MBD_{TLS} from ALS features. The vertical distribution of branch diameters could then be used to describe the crown development and the respective transition from juvenile to mature wood.

The estimations of wood properties could be used to improve

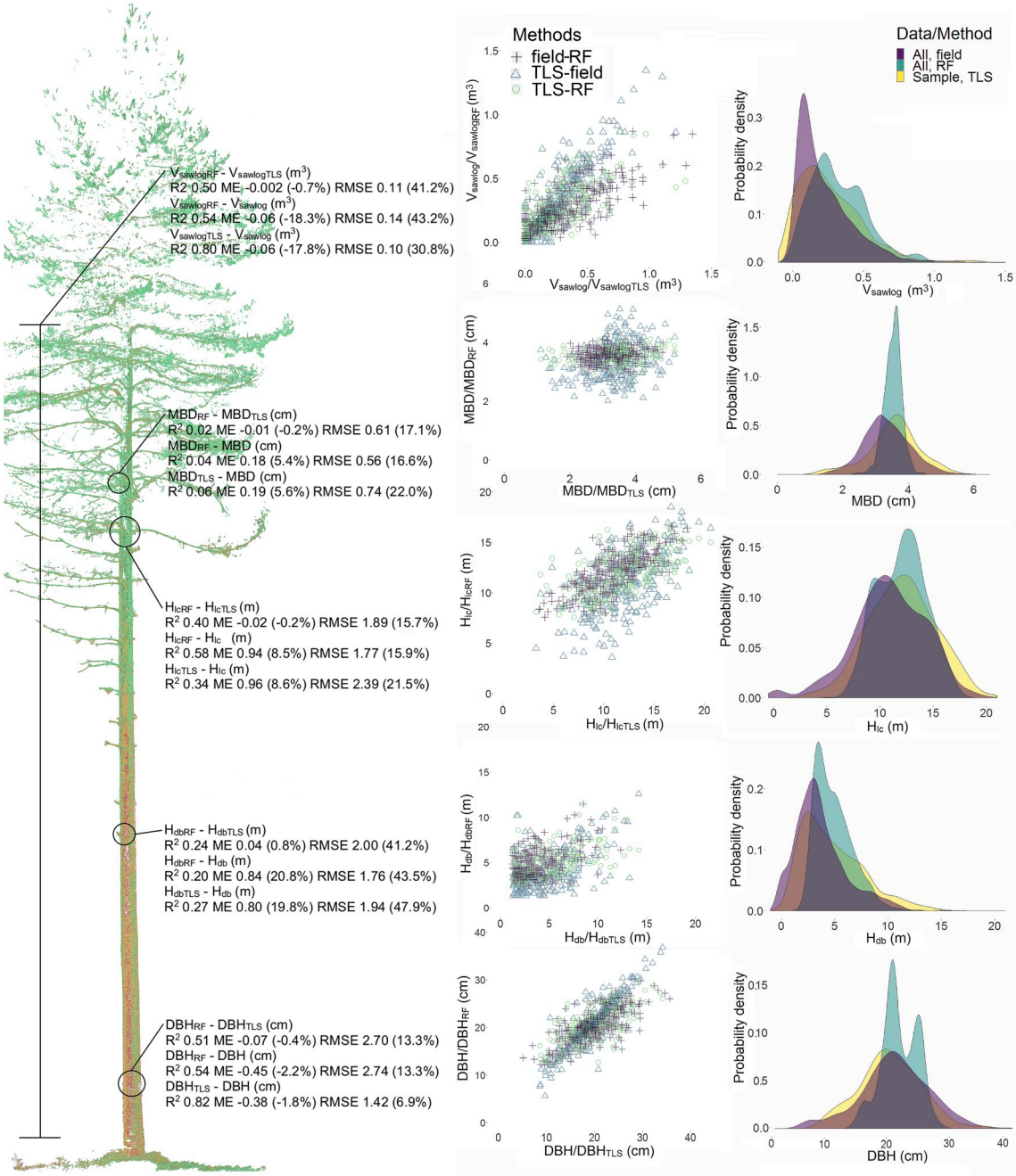

Fig. 7. Comparison of wood quality indicator estimations from terrestrial laser scanning (TLS) point cloud tree models (subscript TLS) with Random Forest predictions based on airborne laser scanning features (subscript RF) and field measurements (no subscript): diameter at breast height (*DBH*), height of the lowest dead branch (H_{db}), height of the live crown base (H_{lc}), maximum branch diameter (*MBD*), and volume of the sawlog section (V_{sawlog}).

decision-making in forestry. Forest management practices that aim to regulate the crown size, e.g., high initial stocking density and delayed thinning, can improve wood quality (Höwler et al., 2017; Huuskonen et al., 2014; Mäkinen, 1999; Mäkinen and Hein, 2006; Weiskittel et al., 2007). However, these forest management options entail prolonged rotations (Dobner et al., 2018; Downes et al., 2002; Fischer et al., 2016), which increases the opportunity costs at the end of the rotation (in volume-centric wood markets). Therefore, some studies proposed wood quality based sale premiums to encourage forest managers and owners to prolong rotations (Malinen et al., 2010; Moore and Cown, 2015). Such policies suppose systems such as those explored in this study to monitor changes in wood quality and quantity over geographic regions and time, as well as means to precisely plan the wood procurement and distribution among various processors, accordingly.

The ALS and especially TLS used in this study are currently considered to be expensive alternatives when acquiring data over larger areas. The availability of data from various sensors and platforms (from mobile laser scanning to satellite imagery) that are dense and accurate enough, as well as developments in algorithms and computing power to process the data, thus require further addressing. This study was undertaken in a region where the mapped areas are relatively small and consist of mostly managed forests (e.g., Scandinavia) and where the integration of such practices to national forest inventories and industrial wood procurement are already underway. However, the precise mapping of natural resources (timber) will play a globally major role in accounting for the various feedbacks between land use (forestry),

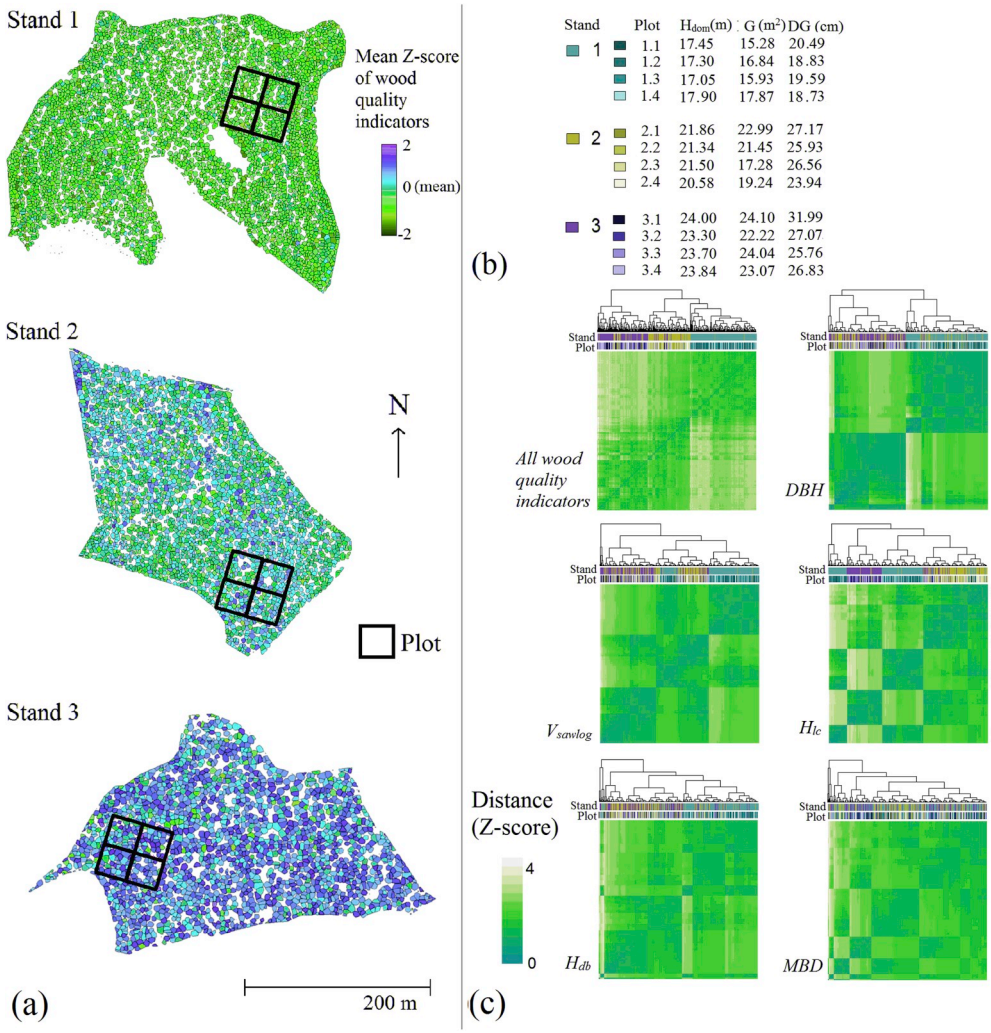

Fig. 8. (a) Tree maps of the three stands studied. Tree crowns are delineated from the airborne laser scanning point clouds, and trees are color-coded based on the mean z-score of wood quality indicators predicted based on terrestrial laser scanning sample trees and using Random Forest. The rectangles indicate the sample plot locations in each stand. (b) Sample plot information from each stand. H_{dom} is the dominant height, G the basal area, and DG the basal-area weighted mean diameter of trees in each subsample. (c) Hierarchically clustered distance matrices of tree-specific wood quality indicator z-scores and the sum of all wood quality indicator z-scores from the sample plots (number of trees, i.e., number of rows and columns 434). Each cell corresponds to the difference in the particular z-score between two trees. The difference (distance) is indicated by the cell color gradient. Dendrograms illustrate the hierarchy of the clusters, with the height in the hierarchy corresponding to the Euclidean distance between z-scores. The horizontal sidebars above the matrices indicate the stand and plot identity of each tree, as color-coded in (b).

ecosystem functioning (wood formation), the environment, and climate (Cardinale et al., 2012; Foley et al., 2005). For example, many regions of temperate and tropical forests are under the threat of forest degradation or deforestation due to the climate change and unsustainable forest management (Sasaki and Putz, 2009). We have described how the ability to map and model wood quality would help to target the harvests more precisely and to, e.g. prolong the rotations in managed forests with possibly positive implications for the sustainability of the commercial forestry, especially in threatened regions.

6. Conclusions

Our study highlighted that TLS point cloud based geometric tree models and ALS crown features can predict stem and crown size from tree- and stand-level factors. These variables can be used as indicators of several size-dependent wood properties that are related to the transition from juvenile to mature wood. The fusion of TLS and ALS could thus make it possible to distinguish between forest stands with distinct carbon sequestration capacity and wood quality, and could be applied to the planning of forest management and use. Our results were based on simple stem and crown variables in specific forest conditions with restricted sample size and they should be applied with the *proviso* that TLS data accurately represent the variability of tree morphologies in the area of interest and that the ALS data are dense and detailed enough for the delineation of individual tree crowns. Approaches such as those presented in this study are part of the transition to precision forestry that is required to enhance sustainable management and use of forest resources.

Acknowledgments

We acknowledge the field crew (Ville Luoma, Aapo Lindberg, Atte Saukkola, Juhani Siivonen, Jussi Kettula, Satulotta Ansiomäki, Kalle Greis, Aimad El-Issaoui, Miska Kauppinen, Topi Rikkinen, and Iikka Haikarainen) for acquiring the sample plot field measurements, geographical reference measurements, and TLS data. The Evo Campus of Häme University of Applied Sciences is acknowledged for providing their facilities, the sample plots, and stand-wise forest inventory data for our use. This work was supported by financial aid received from the Academy of Finland projects [272195] and [315079], the Ministry of Agriculture and Forestry of Finland project [OH300-S42100-03], and Jenny ja Antti Wihurin rahasto. Language was edited by Cathryn Primrose-Mathisen.

Appendix A. Supplementary data

Supplementary data to this article can be found online at https://doi.org/10.1016/j.rse.2019.111474.

Appendix I

The calculation of sawlog volume (V_{sawlog})

Firstly, 1982 Firstly, the following stem diameters (m) were derived with a stem taper equation (Laasasenaho, 1982):

$$D_{20} = DBH * \left[b_0\left(1-\frac{1.3}{H}\right) + b_1\left(1-\frac{1.3}{H}\right)^2 + b_2\left(1-\frac{1.3}{H}\right)^3 + b_3\left(1-\frac{1.3}{H}\right)^5 + b_4\left(1-\frac{1.3}{H}\right)^8 + b_5\left(1-\frac{1.3}{H}\right)^{13} + b_6\left(1-\frac{1.3}{H}\right)^{21} + b_7\left(1-\frac{1.3}{H}\right)^{34} \right]^{-1} \tag{2}$$

$$D_0 = D_{20} * \left[b_0\left(1-\frac{H_0}{H}\right) + b_1\left(1-\frac{H_0}{H}\right)^2 + b_2\left(1-\frac{H_0}{H}\right)^3 + b_3\left(1-\frac{H_0}{H}\right)^5 + b_4\left(1-\frac{H_0}{H}\right)^8 + b_5\left(1-\frac{H_0}{H}\right)^{13} + b_6\left(1-\frac{H_0}{H}\right)^{21} + b_7\left(1-\frac{H_0}{H}\right)^{34} \right] \tag{3}$$

$$D_{sawlog} = D_{20} * \left[b_0\left(1-\frac{H_{sawlog}}{H}\right) + b_1\left(1-\frac{H_{sawlog}}{H}\right)^2 + b_2\left(1-\frac{H_{sawlog}}{H}\right)^3 + b_3\left(1-\frac{H_{sawlog}}{H}\right)^5 + b_4\left(1-\frac{H_{sawlog}}{H}\right)^8 + b_5\left(1-\frac{H_{sawlog}}{H}\right)^{13} + b_6 \left(1-\frac{H_{sawlog}}{H}\right)^{21} + b_7\left(1-\frac{H_{sawlog}}{H}\right)^{34} \right] \tag{4}$$

Then, V_{sawlog} (m^3) was calculated as the volume of truncated cone:

$$Vsawlog = H_{sawlog} * \frac{\pi * \left(\frac{D_0}{2}\right)^2 + \sqrt{\pi * \left(\frac{D_0}{2}\right)^2 * \pi * \left(\frac{D_{sawlog}}{2}\right)^2} + \pi * \left(\frac{D_{sawlog}}{2}\right)^2}{3} \tag{5}$$

Where:

- H is the total tree height (m), measured in field
- DBH is the stem diameter (m) at breast height (1.3 m from ground), measured in field
- D_{20} is the stem diameter (m) at the height of 0.2 * H,
- H_0 is the stump height (m) (assumed 0.2 m in this study)
- D_0 is the stem diameter (m) at H_0,
- D_{sawlog} is the stem diameter (m) at the top of the sawlog section (minimum allowed 0.15 m)
- H_{sawlog} is the height (m) at the top of the sawlog section, solved for D_{sawlog} = 0.15 m
- $b_{0...7}$ are the parameter coefficients from Laasasenaho (1982):
  - $b_0 = 2.1288$
  - $b_1 = -0.6316$
  - $b_2 = -1.6082$
  - $b_3 = 2.4886$
  - $b_4 = -2.4147$
  - $b_5 = 2.3619$
  - $b_6 = -1.7539$
  - $b_7 = 1.0817$

Appendix II

The calculation of maximum branch diameter (MBD)

The following equations were used, applying the methods in Mäkinen and Colin (1998):

$$MBA = e^{b_0 + b_1 * DBH + b_2 * \ln\frac{H-H_{lc}}{0.3} + b_3 * DBH * \ln\frac{H-H_{lc}}{0.3}} + e^{\frac{\mu+\varepsilon}{2}} \tag{6}$$

$$MBD = e^{b_4 + b_5 * DBH + b_6\frac{H_{lc}}{H} + b_7 * \frac{H-H_{lc}}{0.3} + b_8 * \ln\frac{H-H_{lc}}{0.3} + b_9 MBA} + e^{\frac{\mu+\varepsilon}{2}} \tag{7}$$

Where:

- DBH is the stem diameter (m) at breast height (1.3 m), measured in the field
- H is the total tree height (m), measured in the field
- H_{lc} is the height of the live crown base (m), measured in the field
- MBA is the insertion angle (°) associated with MBD
- $\frac{H-H_{lc}}{0.3}$ is the estimate for the number of the whorl of MBD from stem apex
  - MBD is assumed to be found at H_{lc}, based on, e.g. Maguire et al., (1999).bib_Maguire_et_al_1999
  - 0.3 m is assumed the mean whorl-to-whorl distance, based on Pyörälä et al., (2018a).bib_Pyörälä_et_al_2018a
- $b_{0...9}$ are the parameter coefficients from Mäkinen and Colin (1998):
  - $b_0 = 3.8690$
  - $b_1 = -0.0005$
  - $b_2 = 0.1772$
  - $b_3 = -0.0002$
  - $b_4 = 1.9872$

- $b_5 = 0.0012$
- $b_6 = 1.3216$
- $b_7 = -0.0155$
- $b_8 = 0.6781$
- $b_9 = -0.0285$

- $e^{\frac{\mu+\varepsilon}{2}}$ is a correction term calculated with the error coefficients μ and ε from Mäkinen and Colin (1998):
  - $\mu = 0.00702$
  - $\varepsilon = 0.03798$

References

Åkerblom, M., Raumonen, P., Mäkipää, R., Kaasalainen, M., 2017. Automatic tree species recognition with quantitative structure models. Remote Sens. Environ. 191, 1–12.

Aubry-Kientz, M., Dutrieux, R., Ferraz, A., Saatchi, S., Hamraz, H., Williams, J., et al., 2019. A comparative assessment of the performance of individual tree crowns delineation algorithms from ALS data in tropical forests. Remote Sens-Basel 11 (9), 1086.

Auty, D., Moore, J., Achim, A., Lyon, A., Mochan, S., Gardiner, B., 2018. Effects of early respacing on the density and microfibril angle of Sitka spruce wood. Forestry: Int. J. Financ. Res. 91 (3), 307–319.

Axelsson, P., 2000. DEM generation from laser scanner data using adaptive TIN models. Int. Arch. Photogramm. Remote Sens. 33 (4), 111–117.

Barbeito, I., Dassot, M., Bayer, D., Collet, C., Drössler, L., Löf, M., et al., 2017. Terrestrial laser scanning reveals differences in crown structure of Fagus sylvatica in mixed vs. pure European forests. For. Ecol. Manag. 405, 381–390.

Björklund, L., 1997. The interior knot structure of Pinus sylvestris stems. Scand. J. For. Res. 12 (4), 403–412.

Blanchette, D., Fournier, R.A., Luther, J.E., Côté, J.-F., 2015. Predicting wood fiber attributes using local-scale metrics from terrestrial LiDAR data: a case study of Newfoundland conifer species. For. Ecol. Manag. 347, 116–129.

Breiman, L., 2001. Random forests. Mach. Learn. 45 (1), 5–32.

Breiman, L., Friedman, J., Olshen, R., 1984. Classification and Regression Trees. Wadsworth, Belmont, California.

Bucksch, A., Lindenbergh, R., 2008. CAMPINO—a skeletonization method for point cloud processing. Isprs J Photogramm 63 (1), 115–127.

Burt, A., Disney, M., Calders, K., 2018. Extracting Individual Trees from Lidar Point Clouds Using Treeseg. Methods in Ecology and Evolution.

Cardinale, B.J., Duffy, J.E., Gonzalez, A., Hooper, D.U., Perrings, C., Venail, P., et al., 2012. Biodiversity loss and its impact on humanity. Nature 486 (7401), 59.

Chasmer, L., Hopkinson, C., Treitz, P., 2006. Investigating laser pulse penetration through a conifer canopy by integrating airborne and terrestrial lidar. Can. J. Remote Sens. 32 (2), 116–125.

Dalponte, M., Coomes, D.A., 2016. Tree-centric mapping of forest carbon density from airborne laser scanning and hyperspectral data. Methods Ecol. Evol. 7 (10), 1236–1245.

Dassot, M., Constant, T., Fournier, M., 2011. The use of terrestrial LiDAR technology in forest science: application fields, benefits and challenges. Ann. For. Sci. 68 (5), 959–974.

de Conto, T., Olofsson, K., Görgens, E.B., Rodriguez, L.C.E., Almeida, G., 2017. Performance of stem denoising and stem modelling algorithms on single tree point clouds from terrestrial laser scanning. Comput. Electron. Agric. 143, 165–176.

Dobner, M., Huss, J., Tomazello Filho, M., 2018. Wood density of loblolly pine trees as affected by crown thinnings and harvest age in southern Brazil. Wood Sci. Technol. 52 (2), 465–485.

Downes, G.M., Wimmer, R., Evans, R., 2002. Understanding wood formation: gains to commercial forestry through tree-ring research. Dendrochronologia 20 (1–2), 37–51.

Du, P., Kibbe, W.A., Lin, S.M., 2006. Improved peak detection in mass spectrum by incorporating continuous wavelet transform-based pattern matching. Bioinformatics 22 (17), 2059–2065.

Edelsbrunner, H., Mücke, E.P., 1994. Three-dimensional alpha shapes. ACM Trans. Graph. 13 (1), 43–72.

Fischer, C., Høibø, O.A., Vestøl, G.I., Hauglin, M., Hansen, E.H., Gobakken, T., 2018. Predicting dynamic modulus of elasticity of Norway spruce structural timber by forest inventory, airborne laser scanning and harvester-derived data. Scand. J. For. Res. 33 (6), 603–612.

Fischer, C., Vestøl, G.I., Høibø, O., 2016. Modelling the variability of density and bending properties of Norway spruce structural timber. Can. J. For. Res. 46 (7), 978–985.

Fischler, M.A., Bolles, R.C., 1981. Random sample consensus: a paradigm for model fitting with applications to image analysis and automated cartography. Commun. ACM 24 (6), 381–395.

Foley, J.A., DeFries, R., Asner, G.P., Barford, C., Bonan, G., Carpenter, S.R., et al., 2005. Global consequences of land use. Science 309 (5734), 570–574.

Giroud, G., Schneider, R., Fournier, R.A., Luther, J.E., Martin-Ducup, O., 2019. Modeling black spruce wood fiber attributes with terrestrial laser scanning. Can. J. For. Res. 49 (6), 661–669 (ja).

Gorte, B., Pfeifer, N., 2004. Structuring laser-scanned trees using 3D mathematical morphology. Int. Arch. Photogramm. Remote Sens. 35 (B5), 929–933.

Groot, A., Schneider, R., 2011. Predicting maximum branch diameter from crown dimensions, stand characteristics and tree species. For. Chron. 87 (4), 542–551.

Hancock, S., Anderson, K., Disney, M., Gaston, K.J., 2017. Measurement of fine-spatial-resolution 3D vegetation structure with airborne waveform lidar: calibration and validation with voxelised terrestrial lidar. Remote Sens. Environ. 188, 37–50.

Haus, S., 2018. Climate Impact of the Sustainable Use of Forest Biomass in Energy and Material System: a Life Cycle Perspective. Linnaeus University Press.

Hilker, T., Coops, N.C., Newnham, G.J., van Leeuwen, M., Wulder, M.A., Stewart, J., et al., 2012. Comparison of terrestrial and airborne LiDAR in describing stand structure of a thinned lodgepole pine forest. J. For. 110 (2), 97–104.

Hilker, T., Frazer, G.W., Coops, N.C., Wulder, M.A., Newnham, G.J., Stewart, J.D., et al., 2013. Prediction of wood fiber attributes from LiDAR-derived forest canopy indicators. For. Sci. 59 (2), 231–242.

Hilker, T., van Leeuwen, M., Coops, N.C., Wulder, M.A., Newnham, G.J., Jupp, D.L., et al., 2010. Comparing canopy metrics derived from terrestrial and airborne laser scanning in a Douglas-fir dominated forest stand. Trees (Berl.) 24 (5), 819–832.

Holopainen, M., Vastaranta, M., Hyyppä, J., 2014. Outlook for the next generation's precision forestry in Finland. Forests 5 (7), 1682–1694.

Hosonuma, N., Herold, M., De Sy, V., De Fries, R.S., Brockhaus, M., Verchot, L., et al., 2012. An assessment of deforestation and forest degradation drivers in developing countries. Environ. Res. Lett. 7 (4), 044009.

Höwler, K., Annighöfer, P., Ammer, C., Seidel, D., 2017. Competition improves quality-related external stem characteristics of Fagus sylvatica. Can. J. For. Res. 47 (12), 1603–1613.

Huuskonen, S., Hakala, S., Mäkinen, H., Hynynen, J., Varmola, M., 2014. Factors influencing the branchiness of young Scots pine trees. Forestry 87 (2), 257–265.

Hyyppä, J., Inkinen, M., 1999. Detecting and estimating attributes for single trees using laser scanner. Photogramm. J. Finl. 16 (2), 27–42.

Jokela, E.J., Martin, T.A., Vogel, J.G., 2010. Twenty-five years of intensive forest management with southern pines: important lessons learned. J. For. 108 (7), 338–347.

Kankare, V., Joensuu, M., Vauhkonen, J., Holopainen, M., Tanhuanpaa, T., Vastaranta, M., et al., 2014. Estimation of the timber quality of Scots pine with terrestrial laser scanning. Forests 5 (8), 1879–1895.

Korpela, I., Ørka, H.O., Maltamo, M., Tokola, T., Hyyppä, J., 2010. Tree species classification using airborne LiDAR–effects of stand and tree parameters, downsizing of training set, intensity normalization, and sensor type. Silva Fenn. 44 (2), 319–339.

Kuprevicius, A., Auty, D., Achim, A., Caspersen, J.P., 2013. Quantifying the influence of live crown ratio on the mechanical properties of clear wood. Forestry 86 (3), 361–369.

Laasasenaho, J., 1982. Taper curve and volume functions for pine, spruce and birch. Commun. Inst. For. Fenn. 108, 1–74.

Lafarge, T., Pateiro-Lopez, B., 2017. alphashape3d: Implementation of the 3D Alpha-Shape for the Reconstruction of 3D Sets from a Point Cloud. R package version 1.3.

Liang, J., Crowther, T.W., Picard, N., Wiser, S., Zhou, M., Alberti, G., et al., 2016a. Positive biodiversity-productivity relationship predominant in global forests. Science 354 (6309), aaf8957.

Liang, X., Hyyppä, J., Kaartinen, H., Lehtomäki, M., Pyörälä, J., Pfeifer, N., et al., 2018a. International benchmarking of terrestrial laser scanning approaches for forest inventories. Isprs J Photogramm 144, 137–179.

Liang, X., Kankare, V., Hyyppä, J., Wang, Y., Kukko, A., Haggrén, H., et al., 2016b. Terrestrial laser scanning in forest inventories. Isprs J Photogramm 115 (1), 63–77.

Liang, X., Kukko, A., Hyyppä, J., Lehtomäki, M., Pyörälä, J., Yu, X., et al., 2018b. In-situ measurements from mobile platforms: an emerging approach to address the old challenges associated with forest inventories. Isprs J Photogramm 143 (1), 97–107.

Liang, X.L., Kankare, V., Yu, X.W., Hyyppä, J., Holopainen, M., 2014. Automated stem curve measurement using terrestrial laser scanning. IEEE T Geosci Remote 52 (3), 1739–1748.

Liang, X.L., Litkey, P., Hyyppä, J., Kaartinen, H., Vastaranta, M., Holopainen, M., 2012. Automatic stem mapping using single-scan terrestrial laser scanning. IEEE T Geosci Remote 50 (2), 661–670.

Liaw, A., Wiener, M., 2002. Classification and regression by randomForest. In: R News, 6 Ed. 4. pp. 18–22.

Lindberg, E., Holmgren, J., 2017. Individual tree crown methods for 3D data from remote sensing. Curr. For. Res. 3 (1), 19–31.

Lindberg, E., Holmgren, J., Olofsson, K., Olsson, H., 2012. Estimation of stem attributes using a combination of terrestrial and airborne laser scanning. Eur. J. For. Res. 131 (6), 1917–1931.

Lindström, H., 1996. Basic density of Norway spruce. Part II. Predicted by stem taper, mean growth ring width, and factors related to crown development. Wood Fiber Sci. 28 (2), 240–251.

Liu, J., Feng, Z., Yang, L., Mannan, A., Khan, T., Zhao, Z., et al., 2018. Extraction of sample plot parameters from 3D point cloud reconstruction based on combined RTK and CCD continuous photography. Remote Sens-Basel 10 (8), 1299.

Lundqvist, S.-O., Seifert, S., Grahn, T., Olsson, L., García-Gil, M.R., Karlsson, B., et al., 2018. Age and weather effects on between and within ring variations of number, width and coarseness of tracheids and radial growth of young Norway spruce. Eur. J. For. Res. 137 (5), 719–743.

Luther, J.E., Skinner, R., Fournier, R.A., van Lier, O.R., Bowers, W.W., Coté, J.-F., et al., 2014. Predicting wood quantity and quality attributes of balsam fir and black spruce using airborne laser scanner data. Forestry 87 (2), 313–326.
Maas, H.G., Bienert, A., Scheller, S., Keane, E., 2008. Automatic forest inventory parameter determination from terrestrial laser scanner data. Int. J. Remote Sens. 29 (5), 1579–1593.
Macdonald, E., Hubert, J., 2002. A review of the effects of silviculture on timber quality of Sitka spruce. Forestry 75 (2), 107–138.
Maguire, D.A., Johnston, S.R., Cahill, J., 1999. Predicting branch diameters on second-growth Douglas-fir from tree-level descriptors. Can. J. For. Res. 29 (12), 1829–1840.
Mäkinen, H., 1999. Effect of stand density on radial growth of branches of Scots pine in southern and central Finland. Can. J. For. Res. 29 (8), 1216–1224.
Mäkinen, H., Colin, F., 1998. Predicting branch angle and branch diameter of Scots pine from usual tree measurements and stand structural information. Can. J. For. Res. 28 (11), 1686–1696.
Mäkinen, H., Hein, S., 2006. Effect of wide spacing on increment and branch properties of young Norway spruce. Eur. J. For. Res. 125 (3), 239–248.
Malinen, J., Berg, V., Kilpeläinen, H., 2010. Roundwood pricing mechanisms and their performance in Scots pine roundwood markets. Work. Pap. Fin. For. Res. Inst. 147, 35.
Maltamo, M., Karjalainen, T., Repola, J., Vauhkonen, J., 2018. Incorporating tree-and stand-level information on crown base height into multivariate forest management inventories based on airborne laser scanning. Silva Fenn. 52 (3), 1–18.
Maltamo, M., Peuhkurinen, J., Malinen, J., Vauhkonen, J., Packalén, P., Tokola, T., 2009. Predicting tree attributes and quality characteristics of Scots pine using airborne laser scanning data. Silva Fenn. 43 (3), 507–521.
Mansfield, S.D., Parish, R., Goudie, J.W., Kang, K.-Y., Ott, P., 2007. The effects of crown ratio on the transition from juvenile to mature wood production in lodgepole pine in western Canada. Can. J. For. Res. 37 (8), 1450–1459.
Moberg, L., 2006. Predicting knot properties of Picea abies and Pinus sylvestris from generic tree descriptors. Scand. J. For. Res. 21, 48–61.
Moore, J., Achim, A., Lyon, A., Mochan, S., Gardiner, B., 2009. Effects of early re-spacing on the physical and mechanical properties of Sitka spruce structural timber. For. Ecol. Manag. 258 (7), 1174–1180.
Moore, J., Cown, D., 2015. Wood quality variability–what is it, what are the consequences and what we can do about it? J. For. N. Z. 59 (4), 3.
Moore, J.R., Cown, D.J., 2017. Corewood (juvenile wood) and its impact on wood utilisation. Curr. For. Res. 3 (2), 107–118.
Murphy, G.E., Acuna, M.A., Dumbrell, I., 2010. Tree value and log product yield determination in radiata pine (Pinus radiata) plantations in Australia: comparisons of terrestrial laser scanning with a forest inventory system and manual measurements. Can. J. For. Res. 40 (11), 2223–2233.
Næsset, E., Økland, T., 2002. Estimating tree height and tree crown properties using airborne scanning laser in a boreal nature reserve. Remote Sens. Environ. 79 (1), 105–115.
Newnham, G.J., Armston, J.D., Calders, K., Disney, M.I., Lovell, J.L., Schaaf, C.B., et al., 2015. Terrestrial laser scanning for plot-scale forest measurement. Curr. For. Res. 1 (4), 239–251.
Paris, C., Kelbe, D., Van Aardt, J., Bruzzone, L., 2017. A novel automatic method for the fusion of ALS and TLS lidar data for robust assessment of tree crown structure. IEEE T Geosci Remote 55 (7), 3679–3693.
Pretzsch, H., Biber, P., Schütze, G., Kemmerer, J., Uhl, E., 2018. Wood density reduced while wood volume growth accelerated in Central European forests since 1870. For. Ecol. Manag. 429, 589–616.
Pretzsch, H., Rais, A., 2016. Wood quality in complex forests versus even-aged monocultures: review and perspectives. Wood Sci. Technol. 50 (4), 845–880.
Pyörälä, J., Kankare, V., Vastaranta, M., Rikala, J., Holopainen, M., Sipi, M., et al., 2018a. Comparison of terrestrial laser scanning and X-ray scanning in measuring Scots pine (Pinus sylvestris L.) branch structure. Scand. J. For. Res. 33 (3), 291–298.
Pyörälä, J., Liang, X., Saarinen, N., Kankare, V., Wang, Y., Holopainen, M., et al., 2018b. Assessing branching structure for biomass and wood quality estimation using terrestrial laser scanning point clouds. Can. J. Remote Sens. 44 (5), 462–475.
Pyörälä, J., Liang, X., Vastaranta, M., Saarinen, N., Kankare, V., Wang, Y., et al., 2018c. Quantitative assessment of Scots pine (Pinus sylvestris L.) whorl structure in a forest environment using terrestrial laser scanning. IEEE J. Sel. Top. Appl. Earth Obs. Remote Sens. 11 (10), 3598–3607.
Rathgeber, C.B., Cuny, H.E., Fonti, P., 2016. Biological basis of tree-ring formation: a crash course. Front. Plant Sci. 7, 734.
Raumonen, P., Casella, E., Calders, K., Murphy, S., Åkerblom, M., Kaasalainen, M., 2015. Massive-scale tree modelling from TLS data. ISPRS Ann. Photogramm. Remote Sens. Spat. Inf. Sci. 2 (3), 189.
Raumonen, P., Kaasalainen, M., Akerblom, M., Kaasalainen, S., Kaartinen, H., Vastaranta, M., et al., 2013. Fast automatic precision tree models from terrestrial laser scanner data. Remote Sens-Basel 5 (2), 491–520.
Roussel, J.-R., Auty, D., 2019. lidR: Airborne LiDAR Data Manipulation and Visualization for Forestry Applications. R package version 2.0.0.
Saarinen, N., Kankare, V., Vastaranta, M., Luoma, V., Pyörälä, J., Tanhuanpää, T., et al., 2017. Feasibility of Terrestrial laser scanning for collecting stem volume information from single trees. Isprs J Photogramm 123, 140–158.
Saarinen, N., Vastaranta, M., Kankare, V., Tanhuanpää, T., Holopainen, M., Hyyppä, J., et al., 2014. Urban-tree-attribute update using multisource single-tree inventory. Forests 5 (5), 1032–1052.
Sasaki, N., Putz, F.E., 2009. Critical need for new definitions of "forest" and "forest degradation" in global climate change agreements. Conserv. Lett. 2 (5), 226–232.
Sorce, C., Giovannelli, A., Sebastiani, L., Anfodillo, T., 2013. Hormonal signals involved in the regulation of cambial activity, xylogenesis and vessel patterning in trees. Plant Cell Rep. 32 (6), 885–898.
Sterman, J., Siegel, L., Rooney-Varga, J., 2018. Does Replacing Coal with Wood Lower CO2 Emissions? Dynamic Lifecycle Analysis of Wood Bioenergy. Environmental Research Letters.
Swatantran, A., Tang, H., Barrett, T., DeCola, P., Dubayah, R., 2016. Rapid, high-resolution forest structure and terrain mapping over large areas using single photon lidar. Sci. Rep. 6, 28277.
Therneau, T., Atkinson, B., 2018. Rpart: Recursive Partitioning and Regression Trees. 4. R package version, pp. 1–13.
Van Leeuwen, M., Hilker, T., Coops, N.C., Frazer, G., Wulder, M.A., Newnham, G.J., et al., 2011. Assessment of standing wood and fiber quality using ground and airborne laser scanning: a review. For. Ecol. Manag. 261 (9), 1467–1478.
Vastaranta, M., Saarinen, N., Kankare, V., Holopainen, M., Kaartinen, H., Hyyppä, J., et al., 2014. Multisource single-tree inventory in the prediction of tree quality variables and logging recoveries. Remote Sens-Basel 6 (4), 3475–3491.
Vauhkonen, J., Packalen, T., 2018. Uncertainties Related to Climate Change and Forest Management with Implications on Climate Regulation in Finland. Ecosystem Services.
Wang, Y., Hyyppä, J., Liang, X., Kaartinen, H., Yu, X., Lindberg, E., et al., 2016. International benchmarking of the individual tree detection methods for modeling 3-D canopy structure for silviculture and forest ecology using airborne laser scanning. IEEE T Geosci Remote 54 (9), 5011–5027.
Wang, Y., Lehtomäki, M., Liang, X., Pyörälä, J., Kukko, A., Jaakkola, A., et al., 2019. Is field-measured tree height as reliable as believed–A comparison study of tree height estimates from field measurement, airborne laser scanning and terrestrial laser scanning in a boreal forest. Isprs J Photogramm 147, 132–145.
Ward, J., 1963. Hierarchical grouping to optimize an objective function AU - ward, Joe H. J. Am. Stat. Assoc. 58 (301), 236–244.
Weiskittel, A.R., Maguire, D.A., Monserud, R.A., 2007. Modeling crown structural responses to competing vegetation control, thinning, fertilization, and Swiss needle cast in coastal Douglas-fir of the Pacific Northwest, USA. For. Ecol. Manag. 245 (1), 96–109.
White, J.C., Tompalski, P., Vastaranta, M., Wulder, M.A., Saarinen, N., Stepper, C., et al., 2017. A Model Development and Application Guide for Generating an Enhanced Forest Inventory Using Airborne Laser Scanning Data and an Area-Based Approach.
Wilkes, P., Lau, A., Disney, M., Calders, K., Burt, A., de Tanago, J.G., et al., 2017. Data acquisition considerations for Terrestrial Laser Scanning of forest plots. Remote Sens. Environ. 196 (1), 140–153.
Xia, S., Wang, C., Pan, F., Xi, X., Zeng, H., Liu, H., 2015. Detecting stems in dense and homogeneous forest using single-scan TLS. Forests 6 (11), 3923–3945.
Xu, Z., Smyth, C.E., Lemprière, T.C., Rampley, G.J., Kurz, W.A., 2018. Climate change mitigation strategies in the forest sector: biophysical impacts and economic implications in British Columbia, Canada. Mitig. Adapt. Strategies Glob. Change 23 (2), 257–290.
Zhang, S., 1995. Effect of growth rate on wood specific gravity and selected mechanical properties in individual species from distinct wood categories. Wood Sci. Technol. 29 (6), 451–465.
Zhong, L., Cheng, L., Xu, H., Wu, Y., Chen, Y., Li, M., 2017. Segmentation of individual trees from TLS and MLS data. IEEE J. Sel. Top. Appl. Earth Obs. Remote Sens. 10 (2), 774–787.
Zobel, B., 1984. The changing quality of the world wood supply. Wood Sci. Technol. 18 (1), 1–17.
Zobel, B.J., Jett, J.B., 2012. Genetics of Wood Production. Springer Science & Business Media.